

Dynamically or Kinetically Controlled? Computational Study of the Mechanisms of Electrophilic Aminoalkenylation of Heteroaromatics with Keteniminium Ions

Pan Zhang and Zhi-Xiang Yu*



Cite This: *J. Org. Chem.* 2024, 89, 4326–4335



Read Online

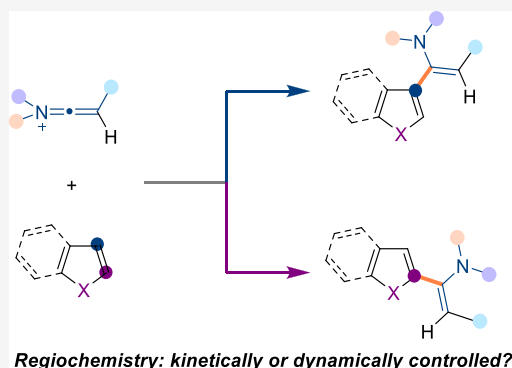
ACCESS |

Metrics & More

Article Recommendations

Supporting Information

ABSTRACT: Quantum chemical calculations and molecular dynamics simulations were applied to study the electrophilic aminoalkenylation of heteroaromatics with keteniminium ions. Post-transition state bifurcation (PTSB) was found in the electrophilic addition step for the aminoalkenylation of pyrroles and indoles, and the selectivity for these reactions was dynamically controlled. However, the aminoalkenylation of furan was kinetically controlled because no apparent PTSB was found in the electrophilic addition step. The substituents on the keteniminium ions can also affect the dynamic results for the aminoalkenylations to pyrroles: the C2-aminoalkenylated product is much more favored over the C3-aminoalkenylated product for keteniminium ions with electron-donating substituents, while the product ratio (C2 product/C3 product) decreased when stronger electron-withdrawing substituents were applied.

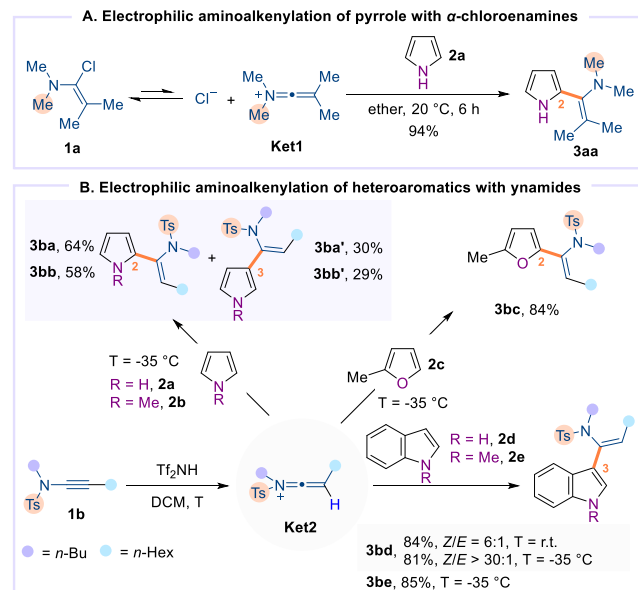


INTRODUCTION

There are three patterns of reaction selectivity control, namely, kinetic, thermodynamic, and dynamic controls.^{1,2} Knowing the exact pattern of selectivity control is important and helpful to understanding these reactions and to designing new reactions in the future. Usually, a reaction's selectivity is controlled by one of these three patterns. In 2023, we discovered that the intramolecular [2 + 2] reaction of keteniminium ions with alkenes has all these three patterns of regiochemistry control,³ depending on the tethers and substituents in the alkene part of the substrates. This is the first reported reaction with three patterns of selectivity control. We were especially surprised by finding the dynamic control existing in the intramolecular [2 + 2] reactions. This also prompted us to consider whether other reactions using keteniminium ions could have different patterns of regiochemistry control if the reaction could give two or more regioisomeric products.

We were attracted by the electrophilic aminoalkenylation reactions of keteniminium ions toward heteroaromatics.⁴ Ghosez et al.^{4a,b} used α -chloroenamines to *in situ* deliver keteniminium ions, which reacted with pyrroles in high regioselectivity and reaction yields (Scheme 1A). However, the reactions of keteniminium ions generated from ynamides, catalyzed by Brønsted acid, were complex: reactions with furans and indoles gave single products, but reactions with pyrroles gave two regioisomeric products (Scheme 1B).^{4c} We hypothesized that the reactions with two regioisomeric products here could also be dynamically controlled while the reactions giving one regioisomeric product could be controlled

Scheme 1. Reported Aminoalkenylation of Heteroaromatics



Received: October 18, 2023

Revised: January 29, 2024

Accepted: February 23, 2024

Published: March 20, 2024



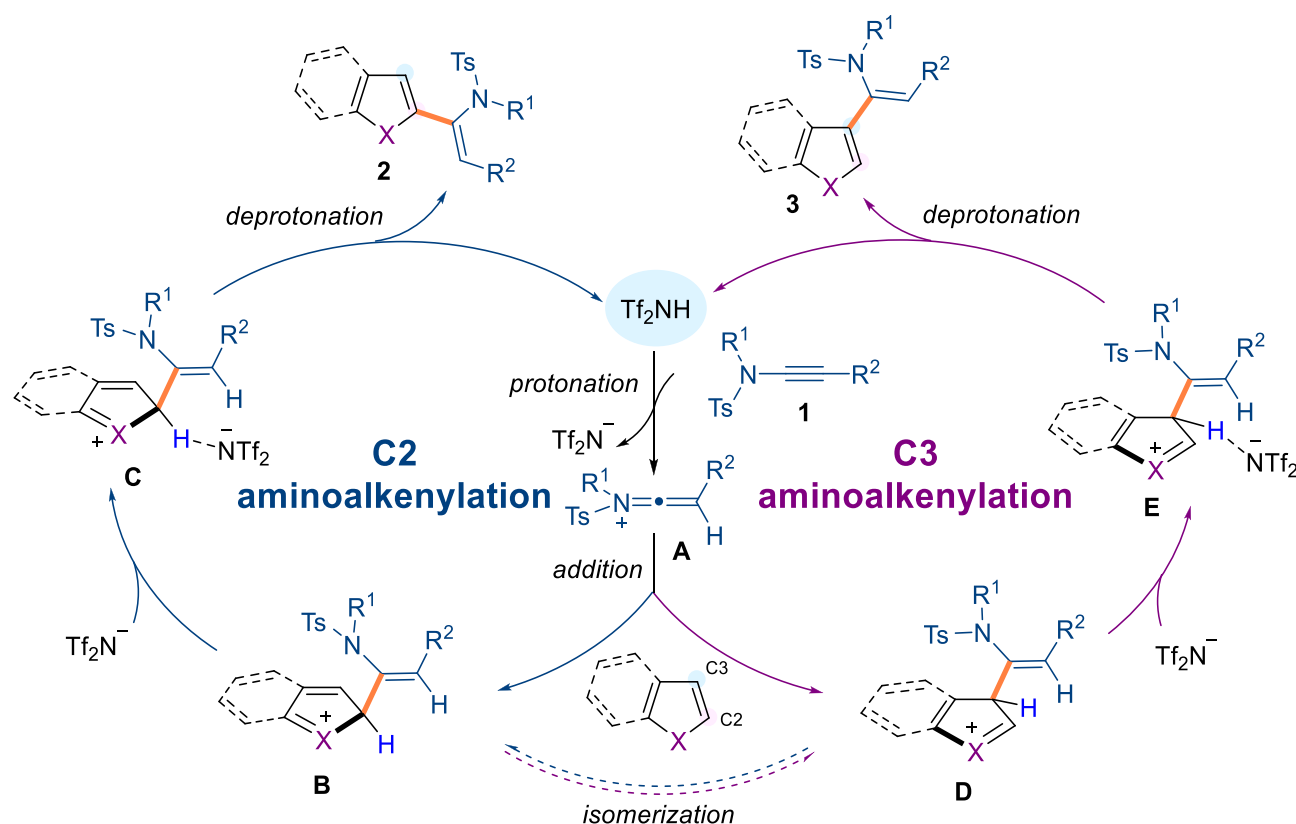


Figure 1. Proposed mechanism for electrophilic aminoalkenylation of heteroaromatics with ynamides.

kinetically (two transition states involved in the regio-determining step could have significant energy difference). We then decided to investigate computationally whether such a hypothesis was correct and the factors influencing the regiochemistry, which are present in this article.

COMPUTATIONAL METHODS

All the DFT calculations were performed using the Gaussian 09 software package.⁵ Pruned integration grids with 99 radial shells and 590 angular points per shell were used. Structure optimizations were performed at the SMD(DCM)⁶/ωB97X-D⁷/def2-SVP⁸ level of theory, unless otherwise specified. The ωB97X-D functional was chosen for its high accuracy in simulating keteniminium ion-related reactions (see the SI for more discussion).³ Unscaled harmonic frequency calculations at the same level were performed to validate each structure as either a minimum or a transition state and to evaluate its zero-point energy and thermal corrections at 298.15 K. Intrinsic reaction coordinate (IRC)⁹ calculations were carried out to confirm the transition states connecting the right reactant(s) and product(s). High-level single-point energies were calculated at the DLPNO-CCSD(T)¹⁰/def2-TZVPP⁸ (with the def2-TZVPP/C¹¹ auxiliary basis set; “TightPNO” and “TightSCF” settings were used) level using the ORCA 4.2.1¹² software package. All of the discussed energy differences were based on Gibbs energies at 298.15 K (standard states are the hypothetical states at 1 mol/L), unless otherwise specified. All the 3D molecular structures were visualized by CYLview.¹³

Molecular orbitals were calculated at the HF¹⁴/6-311G(d)¹⁵ level based on optimized structures. Intrinsic bonding orbital (IBO)¹⁶ analysis was carried out on IboView at the PBE¹⁷/

def2-TZVP⁸ level. Orbital composition analysis with the Ros-Schuit (SCPA) method,¹⁸ noncovalent interaction (NCI) analysis,¹⁹ and conceptual density functional theory (CDFT)²⁰ calculations including condensed Fukui functions were carried out on Multiwfn 3.8dev.²¹ The NCI plot was visualized by VMD 1.9.4a53.²²

Molecular dynamics simulations were performed at the SMD(DCM)/ωB97X-D/def2-SVP or SMD(Et₂O)/ωB97X-D/def2-SVP level of theory, and the temperature was set to be 238.15 K (for hydroarylation of ynamide) or 298.15 K (substituent effect evaluation). Quasi-classical trajectories (QCTs) were initiated from the corresponding transition state regions and propagated forward and backward until either one of the products is formed or the reactants are generated (for criterion and more details, see the SI). The classical equations of motion were integrated with a velocity-Verlet algorithm using Singleton’s program Progdyn,²³ with the energies and derivatives computed on the fly with SMD(DCM)/ωB97X-D/def2-SVP or SMD(Et₂O)/ωB97X-D/def2-SVP using Gaussian 09. The step length for the integration was 1 fs.

RESULTS AND DISCUSSION

Proposed Mechanisms for Electrophilic Aminoalkenylation of Heteroaryls with Keteniminium Ions. Based on the experimental results of electrophilic aminoalkenylation of heteroaromatics with ynamides, we proposed the mechanism shown in Figure 1 to account for the regiochemistry. Ynamide **1** is first protonated by Tf₂NH to give keteniminium ion **A**, which then undergoes electrophilic addition toward the used aromatic molecule. This step leads to two possible cations, namely, C2-alkenylation cation **B** and C3-alkenylation

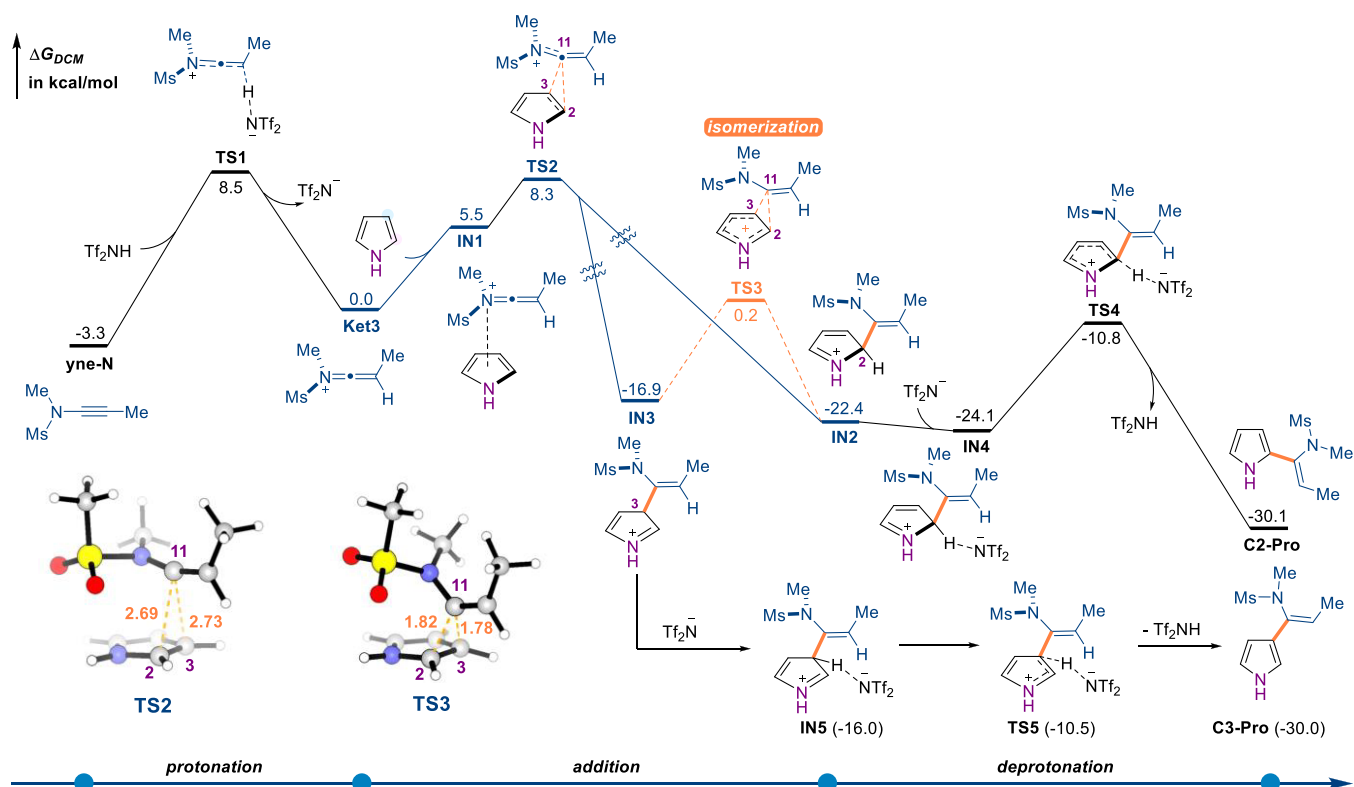


Figure 2. Gibbs energy profile of Brønsted acid-catalyzed electrophilic aminoalkenylation of pyrrole with ynamide **yne-N**. Computed at the DLPNO-CCSD(T)/def2-TZVPP:SMD(DCM)//SMD(DCM)/ ω B97X-D/def2-SVP level. Bond distances are reported in Å.

cation **D**. These two cation intermediates could be in equilibrium via [1,5]-alkenyl shift reaction.^{2c} Finally, deprotonation of intermediates **B** and **D** by the Tf_2N^- affords the final C2-alkenylated and C3-alkenylated products **2** and **3**, respectively. We hypothesized that the regiochemistry for reactions in Scheme 1B is determined by the addition reaction of keteniminium ions toward aromatic molecules.

Mechanism of Electrophilic Aminoalkenylation of Pyrroles. The Gibbs energy profile for aminoalkenylation of pyrrole with the simplified model ynamide **yne-N** is shown in Figure 2. The reaction commences from protonation of **yne-N** by Tf_2NH to generate keteniminium ion **Ket3** via **TS1** (with a computed activation free energy of 11.8 kcal/mol). Pyrrole and **Ket3** then form a cation- π complex **IN1**, which undergoes electrophilic addition via **TS2**, with a quite low activation free energy, 2.8 kcal/mol. Our calculations found that the addition transition state **TS2** is ambimodal,^{1,2} where two intermediates, **IN2** and **IN3**, can be generated. Scanning the C2–C11 and C3–C11 bond distances showed that **TS2** bifurcates to two potential wells of **IN2** and **IN3** (Figure 3A). These two intermediates are connected by the [1,5]-alkenyl shift transition state **TS3**, with an activation free energy of 22.6 kcal/mol (from **IN2** to **TS3**). Subsequently, **IN2** and **IN3** are deprotonated by Tf_2N^- , generating the final products, **C2-Pro** and **C3-Pro**. Because the deprotonation transition states **TS4** and **TS5** are significantly lower in terms of free energy than the transition state **TS3** (interconversion between **IN2** and **IN3**), the reaction selectivity is then determined by the electrophilic addition step of the keteniminium ion to pyrrole. Therefore, the ratio of C2- and C3-aminoalkenylated products is controlled dynamically due to the ambimodal character of **TS2**.

We mention here that the deprotonation process in this reaction could use anions such as Tf_2N^- (we applied this in the present investigation), solvent, or other species. Usually, such a deprotonation is fast and not regio-determining.²⁴ Here, using Tf_2N^- as the deprotonation species demonstrates this claim. Other species could be slower or faster than Tf_2N^- for deprotonation, but this will not change our conclusion that the ambimodal **TS2** determines the regiochemistry. Anion Tf_2N^- could form hydrogen bonding complexes with other species, and the barrier for the deprotonation could be increased. However, this will not change the above conclusion either, because deprotonation transition states are lower than both **TS2** and **TS3**.

To get a quantitative ratio of two regioisomers, QCT molecular dynamics simulations were carried out (Figure 3). We computed 331 trajectories, and among them, 199 trajectories led to **IN2**, 57 trajectories led to **IN3**, and the other 75 recrossed (Figure 3D). Consequently, the ratio of **C2-Pro**/**C3-Pro** was 3.5:1, which was consistent with the experimental observation ($3\text{ba}:3\text{ba}' = 2.1:1$). It is interesting to find that there are four types of representative trajectories: two types of trajectories led to **IN2** and **IN3**, respectively (Figure 3C). For trajectories leading to **IN2**, one first passed through the region of **TS3** and then gave **IN2** with a relatively long lifetime (164 fs for the selected representative trajectory). The other one had a relatively shorter lifetime (134 fs for the selected representative trajectory) without passing through **TS3**. Similarly, there are also two types of trajectories leading to **IN3**: one directly gave **IN3**, and the other one first passed through **TS3** and then afforded **IN3**.

Previously, Houk et al.²⁵ used bond lengths in the ambimodal transition structures to correlate them with the product ratio. Using this model, we predicted that **IN2**/**IN3**

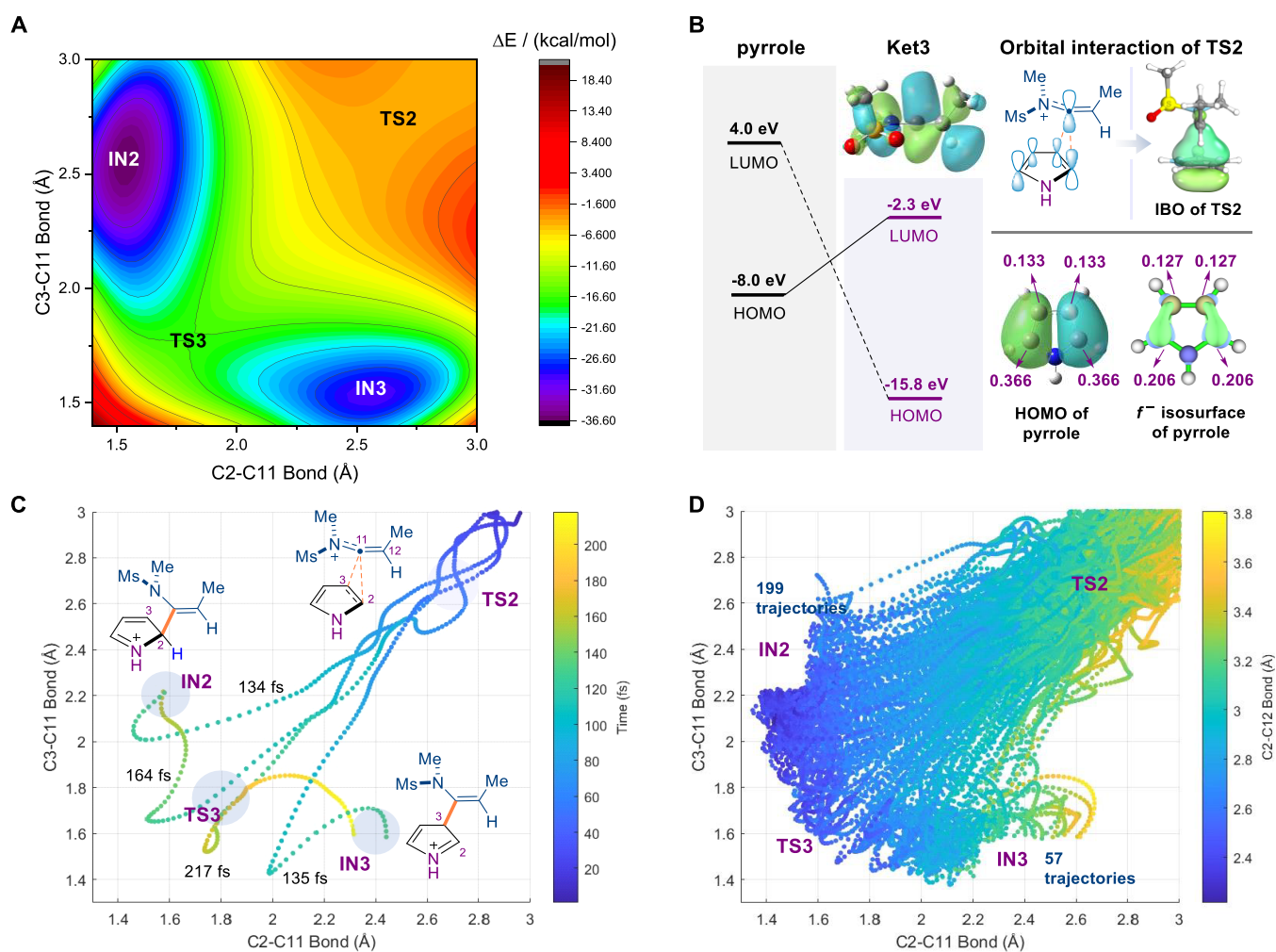


Figure 3. Post-transition state bifurcation of addition of keteniminium ion **Ket3** to pyrrole. (A) Potential energy surface for addition of keteniminium ion **Ket3** to pyrrole. Scanned at the SMD(DCM)/ ω B97X-D/def2-SVP level. (B) Orbital analysis of pyrrole, **Ket3**, and **TS2**. (C) Representative quasi-classical trajectories leading to **IN2** and **IN3**, simulated at 238.15 K. (D) QCTs leading to **IN2** and **IN3** generated in molecular dynamics simulation, simulated at 238.15 K. The composition of the selected atoms in HOMO and the condensed Fukui f^- function of the selected atoms of pyrrole were labeled on the corresponding surfaces.

was 1.5 (calculated from equation $\ln(\text{IN2}/\text{IN3}) = -9.4x$, x is the C2–C11 and C3–C11 bond difference (-0.04 Å) of **TS2**). This prediction was also close to the experimental results.

To understand the post-transition state bifurcation (PTSB) process, we analyzed the frontier orbital of pyrrole and **Ket3**, finding that the major orbital interaction comes from the highest occupied molecular orbital (HOMO) of pyrrole and the lowest unoccupied molecular orbital (LUMO) of **Ket3** (Figure 3B). The LUMO of **Ket3** can interact with both C2 and C3 positions in **TS2**, making the formation of both **IN2** and **IN3** possible, which is also supported by IBO analysis of **TS2**. The interaction of pyrrole's LUMO and **Ket3**'s HOMO is very weak due to the large energy gap between them (19.8 eV).

It should be noted that the [2 + 2] cycloaddition pathway of **Ket3** and pyrrole is kinetically and thermodynamically disfavored, because dearomatization is involved in this pathway (see the SI for details).

Mechanisms of Electrophilic Aminoalkenylation of Indoles and Furans with Keteniminium Ions. Now let us discuss the reaction mechanisms of other aromatic molecules,

indoles and furans, with keteniminium ions. For indole, the addition transition state **TS2-I** is also ambimodal, leading to both **IN2-I** and **IN3-I**, with an activation free energy of 3.6 kcal/mol (from **IN1-I** to **TS2-I**, Figure 4A). These two intermediates are connected by the [1,5]-alkenyl shift transition state **TS3-I**. Similar to aminoalkenylation of pyrrole, **IN2-I** and **IN3-I** undergo a deprotonation process to give their corresponding product via **TS4-I** and **TS5-I**, respectively. Compared with the isomerization process, deprotection of both **IN2-I** and **IN3-I** has much lower activation free energy, indicating that the regiochemistry of the present reaction is determined by the first transition state, the ambimodal **TS2-I**.

QCT molecular dynamics simulations were also performed to evaluate the reaction selectivity quantitatively. We calculated 102 trajectories from **TS2-I**, finding that 90 trajectories of them led to **IN3-I** while only two trajectories led to **IN2-I** (the rest recrossed to give the starting materials). The dynamic simulation predicted high selectivity, preferring to give the C3-alkenylated product. This was consistent with experimental results that only C3-aminoalkenylated products were obtained.

The mechanism of furans with keteniminium ions is different from that of indoles with keteniminium ions (Figure 4B). The

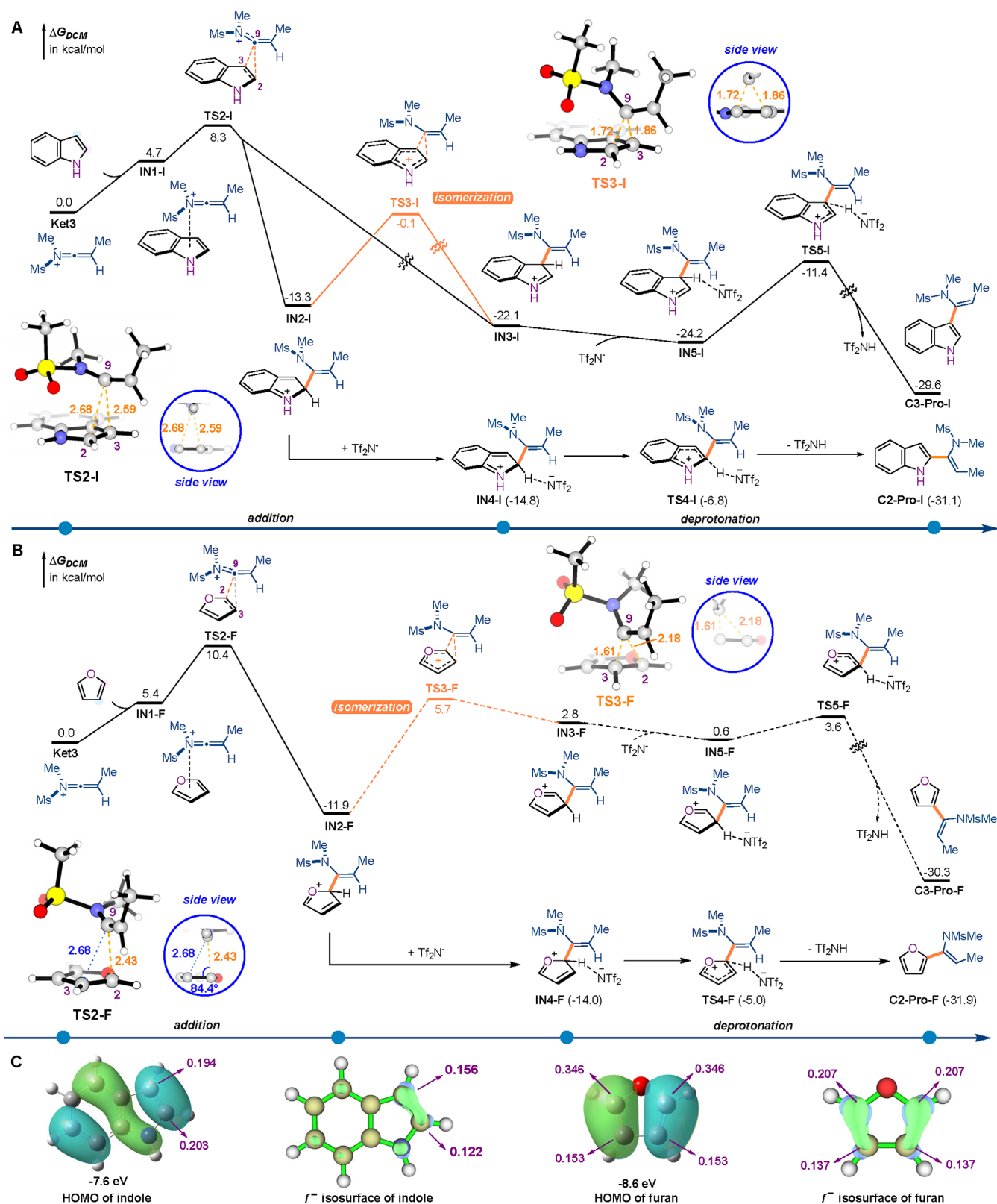


Figure 4. Gibbs energy profile for the addition of the keteniminium ion **Ket3** to indole (A) and furan (B) and surfaces of indole and furan (C). Bond distances are reported in Å. Computed at the DLPNO-CCSD(T)/def2-TZVPP:SMD(DCM)//SMD(DCM)/ ω B97X-D/def2-SVP level. Side view means a perspective perpendicular to the plane of the three-center transition state. The composition of the selected atoms in HOMO and the condensed Fukui f^- function of the selected atoms of indole and furan were labeled on the corresponding surfaces.

addition of keteniminium to furan via **TS2-F** has an activation free energy of 5.0 kcal/mol (from **IN1-F** to **TS2-F**), higher than the required activation free energies of the additions of

keteniminium ion **Ket3** to pyrrole and indole. Relaxed potential energy surface scan confirmed that there is no obvious bifurcation characteristics for **TS2-F** (see the SI).

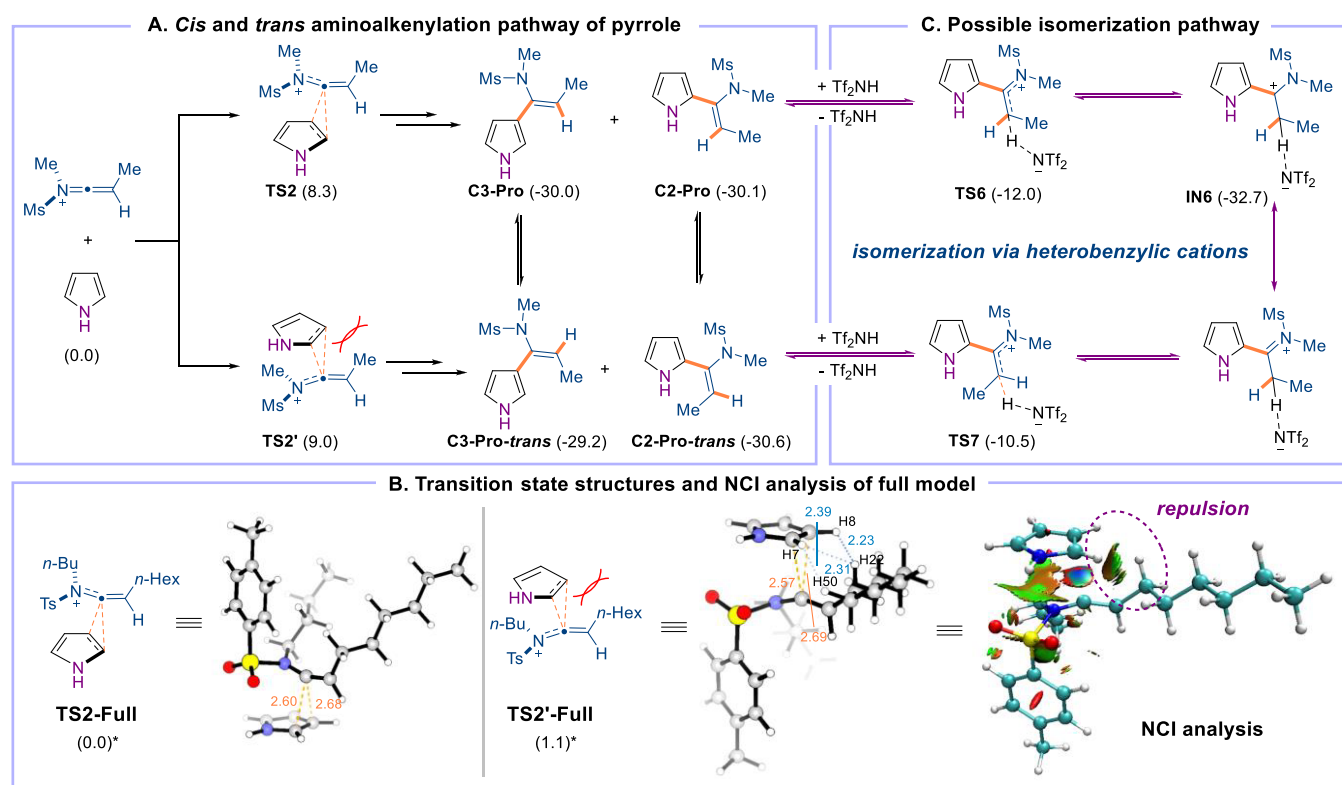


Figure 5. Rationalization for *cis/trans* selectivity of aminoalkenylation of pyrroles. Computed at the DLPNO-CCSD(T)/def2-TZVPP:SMD(DCM)//SMD(DCM)/ ω B97X-D/def2-SVP level. Bond distances are reported in Å. *Computed at the DLPNO-CCSD(T)/def2-TZVPP:SMD(DCM)//SMD(DCM)/ ω B97X-D/def2-TZVP level.

Further dynamics simulations were also applied to quantify the selectivity. We observed 130 trajectories, among 150 simulated trajectories, that led to IN2-F, while 20 trajectories recrossed to give the starting materials. No trajectories were found to give IN3-F, indicating that this reaction was unlikely to be ambimodal. These results infer that the PTSB properties of a reaction may disappear when a reaction component was changed to a similar one: here from pyrrole to furan, the reaction selectivity changed from dynamic control to kinetic control. Such a phenomenon has also been reported by Burns and Boittier,^{2f} who found that the cycloaddition of oxidopyrylium and butadiene is dynamically controlled while cycloaddition of oxidopyridinium and butadiene is absent of a PTSB.

Once generated, IN2-F then forms complex IN4-F with TF_2N^- . Subsequent deprotonation via TS4-F is easy, with an activation free energy of 9.0 kcal/mol leading to C2-Pro-F. The isomerization process giving IN3-F is 10.7 kcal/mol disfavored compared to TS4-F, indicating that formation of the C3-aminoalkenylated product is disfavored, which is consistent with experimental results.

It is interesting to find that there is no apparent correlation between HOMO composition differences (between C2 and C3) and the regioselectivity. As shown in Figures 3B and 4C, the compositions of C2 and C3 in the HOMO are close in both pyrrole (Figure 3B) and furan (Figure 4C), but their reactions with keteniminium ions show significant difference in regioselectivity. Condensed Fukui function f^- could not be applied to explain the selectivity difference either, because f^- values for C2 and C3 of furan and pyrrole are similar. We attribute the above difference to the reactivity of hetero-

aromatics, which in turn leads to the shape change of the potential energy surface. We provide an explanation below.

Addition of Ket3 to furan via TS2-F leads to the C2-alkenylated intermediate IN2-F directly, and no TS was found for electrophilic attack at the C3 position. The reason could be that the former process is exergonic and the latter is endergonic. The possible TS region for electrophilic attack at the C3 position has high energy on the potential energy surface, and its geometry should be similar to TS2-F. Since C3 attack is endergonic, locating such TS would converge at TS2-F. Besides, endergonic reactions usually have late transition states and the possibility of bifurcation could be lower. This can be used to understand why no obvious PTSB was found for electrophilic addition of Ket3 to furan. On the other hand, for pyrrole and indole, both electrophilic attacks at C2 and C3 position are very exergonic, making the potential energy surface suitable for bifurcation. In these cases, PTSBs were found.

Rationalization for *cis*-Aminoalkenylation. The aminoalkenylation reaction of indole toward 3bd shows good *Z/E* (*cis/trans*) selectivity (*Z/E* > 30:1) at a low temperature (-35°C), while only a moderate selectivity (*Z/E* = 6:1) was observed at room temperature (Scheme 1B). We investigated these two processes and found that the addition TS in the *trans*-aminoalkenylation pathway (TS2') giving the *E* product is disfavored by 0.7 kcal/mol, compared to TS2 in the *cis*-aminoalkenylation pathway giving the *Z* product (Figure 5A). The free energy difference could not account for the high *Z/E* selectivity at low temperatures. Besides, the stabilities of the *cis* and *trans* products are almost the same (Figure 5A). In this case, we had to use real reactants to understand the stereochemistry (Figure 5B), finding that *cis*-aminoalkenylation

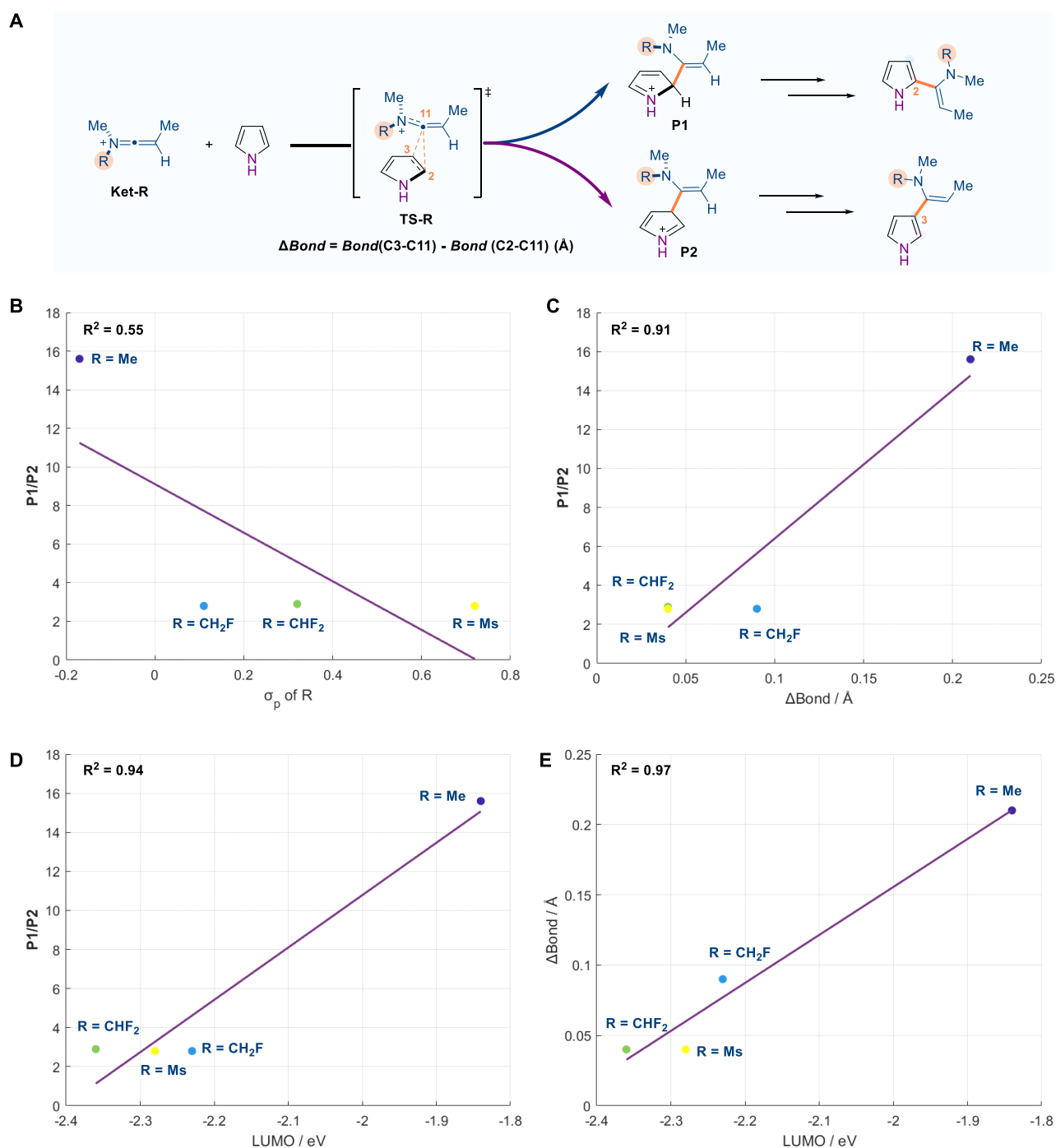


Figure 6. Substitution effects of keteniminium ions for electrophilic aminoalkenylation. Simulations were carried out at 298.15 K using DCM as the solvent.

via **TS2-Full** is 1.1 kcal/mol favored over *trans*-aminoalkenylation via **TS2'-Full**. The *Z/E* ratio was predicted to be 10:1, close to the experimental results. This difference in energy of the two transition states could be attributed to the steric repulsion between the alkyl substitution of the keteniminium ion and the pyrrole ring, as indicated by the short distance of H7–H50, H7–H22, and H8–H22 in **TS2'-Full**, also supported by the NCI analysis of **TS2'-Full**. It is interesting to find that there is an isomerization process between *cis*-product and *trans*-product via heterobenzylic cations, as indicated in **Figure 5C**. **C2-Pro** can be protonated via **TS6**, giving heterobenzylic cation **IN6**, which then

undergoes deprotonation of another H atom by Tf_2N^- , affording **C2-Pro-trans**. The isomerization process with an activation free energy of 22.2 kcal/mol (from **IN6** to **TS7**) at low temperatures is quite slow; thus, the selectivity is determined by the addition transition states (kinetically controlled). At room temperature, this process is much faster and the *Z/E* selectivity is lower because this reaction is thermodynamically controlled.

Substitution Effects of Keteniminium Ions. The computational results presented above illustrate that the electrophilic additions of keteniminium ions to various aromatics have different reaction outcomes. Additionally, the

substituents on the keteniminium ions affect reaction selectivity, as evidenced by the reactions shown in Scheme 1A,B. These results led us to hypothesize that changing the substitutions on keteniminium ions can also modify the outcomes of these dynamically controlled reactions. To test this hypothesis, we varied the R group of Ket-R, from mesyl (Ms), difluoromethyl (CHF₂), and fluoromethyl (CH₂F), to methyl (Me) and then calculated their corresponding transition states (TSs). For those obtained TSs exhibiting ambimodal characteristics, we applied QCT molecular dynamics to predict the reaction selectivity between the C2-alkenylated product (P1) and the C3-alkenylated product (P2) (Figure 6).

When R = Me, the computed P1/P2 is 15.6 and a high selectivity for obtaining the C2-alkenylated product was predicted, aligning well with the experimental outcomes depicted in Scheme 1A (see the SI for more details). In contrast, with R = CH₂F, the predicted ratio of products was 2.8, significantly lower than that observed for the substrate with R = Me. Intriguingly, as the electron-withdrawing ability²⁶ of the R group increases, the selectivity unexpectedly remains relatively constant at around 2.8 (see Figure 6B).

To unravel the origins responsible for the substitution effects on the regioselectivity, we conducted additional analyses. Figure 6C illustrates a good correlation between the regioselectivity of P1/P2 and the difference in bond lengths between C3–C11 and C2–C11. As the $\Delta Bond$ value increases, so does the P1/P2 ratio. Linear regression of P1/P2 against $\Delta Bond$ confirmed this correlation, with a high correlation coefficient (R^2) of 0.91. Similarly, a correlation was identified between P1/P2 and the LUMO energy of Ket-R (Figure 6D). When the LUMO energy increases, the ratio of P1/P2 also increases. Notably, $\Delta Bond$ exhibits a high correlation with the LUMO energy of Ket-R (Figure 6E). Consequently, we conclude that substitutions on keteniminium ions can influence the regioselectivity by modulating the shape of the potential energy surface. When employing Ket-R with a lower LUMO, the electrophilic addition barrier diminishes (lower LUMO means high electrophilicity)²⁷ and the potential energy surface becomes flatter, leading to a convergence of possibilities for forming both products.

CONCLUSIONS

The mechanisms of electrophilic aminoalkenylation of heteroaromatics with keteniminium ions were studied. Quantum chemical calculations revealed that the reaction commenced from protonation of ynamide to generate keteniminium ions, followed by addition of keteniminium ions to aromatics and deprotonation to afford the final products. The interesting regioselectivity between the C2- and C3-alkenylated products is determined by the addition step. Further QCT molecular dynamics studies showed that addition of keteniminium ions to pyrrole has a bifurcating potential energy surface, and consequently, the reaction yields two aminoalkenylated products. Addition of keteniminium ions to indole is also dynamically controlled, with a large dynamic preference for C3-aminoalkenylation. Molecular dynamics simulations not only successfully predicted the distribution of products but also gave the time-resolved mechanism of the reaction. However, no apparent post-transition state bifurcation (PTSB) was found in the addition of keteniminium ions to furan and only one product can be selectively obtained. Importantly, we found that the selectivity

for pyrroles can be adjusted by changing substitutions on keteniminium ions, providing useful information for further reaction design and optimization.

ASSOCIATED CONTENT

Data Availability Statement

The data underlying this study are available in the published article and its supplementary material.

Supporting Information

The Supporting Information is available free of charge at <https://pubs.acs.org/doi/10.1021/acs.joc.3c02379>.

Detailed molecular dynamics simulation methods; more discussions; computed energies of potential energy surface scan; substitution effects of keteniminium ions; computed energies of the stationary points; and Cartesian coordinates of the stationary points (PDF)

AUTHOR INFORMATION

Corresponding Author

Zhi-Xiang Yu – Beijing National Laboratory for Molecular Sciences (BNLMS), Key Laboratory of Bioorganic Chemistry and Molecular Engineering of Ministry of Education, College of Chemistry, Peking University, Beijing 100871, China; orcid.org/0000-0003-0939-9727; Email: yuzx@pku.edu.cn

Author

Pan Zhang – Beijing National Laboratory for Molecular Sciences (BNLMS), Key Laboratory of Bioorganic Chemistry and Molecular Engineering of Ministry of Education, College of Chemistry, Peking University, Beijing 100871, China

Complete contact information is available at:

<https://pubs.acs.org/doi/10.1021/acs.joc.3c02379>

Notes

The authors declare no competing financial interest.

ACKNOWLEDGMENTS

This work was supported by the National Natural Science Foundation of China (21933003) and High-Performance Computing Platform of Peking University.

REFERENCES

- (1) For reviews: (a) Ess, D. H.; Wheeler, S. E.; Iafe, R. G.; Xu, L.; Çelebi-Ölçüm, N.; Houk, K. N. Bifurcations on Potential Energy Surfaces of Organic Reactions. *Angew. Chem., Int. Ed.* **2008**, *47*, 7592–7601. (b) Rehbein, J.; Carpenter, B. K. Do we fully understand what controls chemical selectivity? *Phys. Chem. Chem. Phys.* **2011**, *13*, 20906–20922. (c) Hare, S. R.; Tantillo, D. J. Post-transition state bifurcations gain momentum – current state of the field. *Pure Appl. Chem.* **2017**, *89*, 679–698. (d) McLeod, D.; Thøgersen, M. K.; Jessen, N. I.; Jørgensen, K. A.; Jamieson, C. S.; Xue, X.-S.; Houk, K. N.; Liu, F.; Hoffmann, R. Expanding the Frontiers of Higher-Order Cycloadditions. *Acc. Chem. Res.* **2019**, *52*, 3488–3501. (e) Yang, Z.; Jamieson, C. S.; Xue, X.-S.; Garcia-Borràs, M.; Benton, T.; Dong, X.; Liu, F.; Houk, K. N. Mechanisms and Dynamics of Reactions Involving Entropic Intermediates. *Trends in Chemistry* **2019**, *1*, 22–34. (f) Zhang, K.; Wang, W.; Zhu, H.; Peng, Q. Advances on Quasi-classical Molecular Dynamics of Organic Reaction Mechanisms. *Chin. J. Org. Chem.* **2021**, *41*, 3995–4006.
- (2) For selected examples: (a) Caramella, P.; Quadrelli, P.; Toma, L. An Unexpected Bispericyclic Transition Structure Leading to 4 + 2 and 2 + 4 Cycloadducts in the *Endo* Dimerization of Cyclopentadiene. *J. Am. Chem. Soc.* **2002**, *124*, 1130–1131. (b) Wang, Z. J.; Benitez, D.;

- Tkatchouk, E.; Goddard, W. A., III; Toste, F. D. Mechanistic Study of Gold(I)-Catalyzed Intermolecular Hydroamination of Allenes. *J. Am. Chem. Soc.* **2010**, *132*, 13064–13071. (c) Zhang, L.; Wang, Y.; Yao, Z.-J.; Wang, S.; Yu, Z.-X. Kinetic or Dynamic Control on a Bifurcating Potential Energy Surface? An Experimental and DFT Study of Gold-Catalyzed Ring Expansion and Spirocyclization of 2-Propargyl- β -tetrahydrocarbolines. *J. Am. Chem. Soc.* **2015**, *137*, 13290–13300. (d) Patel, A.; Chen, Z.; Yang, Z.; Gutierrez, O.; Liu, H. – w.; Houk, K. N.; Singleton, D. A. Dynamically Complex [6 + 4] and [4 + 2] Cycloadditions in the Biosynthesis of Spinosyn A. *J. Am. Chem. Soc.* **2016**, *138*, 3631–3634. (e) Chen, S.; Yu, P.; Houk, K. N. Ambimodal Dipolar/Diels–Alder Cycloaddition Transition States Involving Proton Transfers. *J. Am. Chem. Soc.* **2018**, *140*, 18124–18131. (f) Burns, J. M.; Boittier, E. D. Pathway Bifurcation in the (4 + 3)/(5 + 2)-Cycloaddition of Butadiene and Oxidopyrylium Ylides: The Significance of Molecular Orbital Isosymmetry. *J. Org. Chem.* **2019**, *84*, 5997–6005. (g) Xue, X.-S.; Jamieson, C. S.; Garcia-Borràs, M.; Dong, X.; Yang, Z.; Houk, K. N. Ambimodal Trispericyclic Transition State and Dynamic Control of Periselectivity. *J. Am. Chem. Soc.* **2019**, *141*, 1217–1221. (h) Feng, Z.; Tantillo, D. J. Dynamic Effects on Migratory Aptitudes in Carbocation Reactions. *J. Am. Chem. Soc.* **2021**, *143*, 1088–1097. (i) Zhang, H.; Novak, A. J. E.; Jamieson, C. S.; Xue, X.-S.; Chen, S.; Trauner, D.; Houk, K. N. Computational Exploration of the Mechanism of Critical Steps in the Biomimetic Synthesis of Preusolactone A, and Discovery of New Ambimodal (5 + 2)/(4 + 2) Cycloadditions. *J. Am. Chem. Soc.* **2021**, *143*, 6601–6608. (j) Jamieson, C. S.; Sengupta, A.; Houk, K. N. Cycloadditions of Cyclopentadiene and Cycloheptatriene with Tropones: All *Endo*-[6 + 4] Cycloadditions Are Ambimodal. *J. Am. Chem. Soc.* **2021**, *143*, 3918–3926. (k) Yang, B.; Schouten, A.; Ess, D. H. Direct Dynamics Trajectories Reveal Nonstatistical Coordination Intermediates and Demonstrate that σ and π -Coordination Are Not Required for Rhenium(I)-Mediated Ethylene C–H Activation. *J. Am. Chem. Soc.* **2021**, *143*, 8367–8374. (l) Wang, X.; Zhang, C.; Jiang, Y.; Wang, W.; Zhou, Y.; Chen, Y.; Zhang, B.; Tan, R. X.; Ge, H. M.; Yang, Z. J.; Liang, Y. Influence of Water and Enzyme on the Post-Transition State Bifurcation of NgnD-Catalyzed Ambimodal [6 + 4]/[4 + 2] Cycloaddition. *J. Am. Chem. Soc.* **2021**, *143*, 21003–21009. (m) Zhang, C.; Wang, X.; Chen, Y.; He, Z.; Yu, Y.; Liang, Y. Dynamical Trajectory Study of the Transannular [6 + 4] and Ambimodal Cycloaddition in the Biosynthesis of Heronamides. *J. Org. Chem.* **2020**, *85*, 9440–9445. (n) Lee, S.; Goodman, J. M. Rapid Route-Finding for Bifurcating Organic Reactions. *J. Am. Chem. Soc.* **2020**, *142*, 9210–9219.
- (3) Zhang, P.; Yu, Z.-X. Kinetic, Thermodynamic, and Dynamic Control in Normal vs. Cross [2 + 2] Cycloadditions of Ene-Keteniminium Ions: Computational Understanding, Prediction, and Experimental Verification. *J. Am. Chem. Soc.* **2023**, *145*, 9634–9645.
- (4) For selected examples: (a) Marchand-Brynaert, J.; Ghosez, L. Electrophilic aminoalkenylation of aromatics with α -chloroenamines. *J. Am. Chem. Soc.* **1972**, *94*, 2869. (b) Ghosez, L. α -Chloroenamines: New Reagents for Organic Synthesis. *Angew. Chem., Int. Ed. Engl.* **1972**, *11*, 852–853. (c) Zhang, Y. Synthesis of vinylpyrroles, vinylfurans and vinylindoles via a Brønsted acid catalyzed highly regio- and stereoselective *cis*-hydroarylation of ynamides. *Tetrahedron* **2006**, *62*, 3917–3927.
- (5) Frisch, M. J.; Trucks, G. W.; Schlegel, H. B.; Scuseria, G. E.; Robb, M. A.; Cheeseman, J. R.; Scalmani, G.; Barone, V.; Mennucci, B.; Petersson, G. A.; Nakatsuji, H.; Caricato, M.; Li, X.; Hratchian, H. P.; Izmaylov, A. F.; Bloino, J.; Zheng, G.; Sonnenberg, J. L.; Hada, M.; Ehara, M.; Toyota, K.; Fukuda, R.; Hasegawa, J.; Ishida, M.; Nakajima, T.; Honda, Y.; Kitao, O.; Nakai, H.; Vreven, T.; Montgomery, J. A., Jr.; Peralta, J. E.; Ogliaro, F.; Bearpark, M.; Heyd, J. J.; Brothers, E.; Kudin, K. N.; Staroverov, V. N.; Keith, T.; Kobayashi, R.; Normand, J.; Raghavachari, K.; Rendell, A.; Burant, J. C.; Iyengar, S. S.; Tomasi, J.; Cossi, M.; Rega, N.; Millam, J. M.; Klene, M.; Knox, J. E.; Cross, J. B.; Bakken, V.; Adamo, C.; Jaramillo, J.; Gomperts, R.; Stratmann, R. E.; Yazyev, O.; Austin, A. J.; Cammi, R.; Pomelli, C.; Ochterski, J. W.; Martin, R. L.; Morokuma, K.;
- Zakrzewski, V. G.; Voth, G. A.; Salvador, P.; Dannenberg, J. J.; Dapprich, S.; Daniels, A. D.; Farkas, Ö.; Foresman, J. B.; Ortiz, J. V.; Cioslowski, J.; Fox, D. J. *Gaussian 09, Revision E.01*; Gaussian, Inc.: Wallingford, CT, 2013.
- (6) Marenich, A. V.; Cramer, C. J.; Truhlar, D. G. Universal Solvation Model Based on Solute Electron Density and on a Continuum Model of the Solvent Defined by the Bulk Dielectric Constant and Atomic Surface Tensions. *J. Phys. Chem. B* **2009**, *113*, 6378–6396.
- (7) Chai, J.-D.; Head-Gordon, M. Long-range corrected hybrid density functionals with damped atom-atom dispersion corrections. *Phys. Chem. Chem. Phys.* **2008**, *10*, 6615–6620.
- (8) Weigend, F.; Ahlrichs, R. Balanced basis sets of split valence, triple zeta valence and quadruple zeta valence quality for H to Rn: Design and assessment of accuracy. *Phys. Chem. Chem. Phys.* **2005**, *7*, 3297–3305.
- (9) Fukui, K. The path of chemical reactions - the IRC approach. *Acc. Chem. Res.* **1981**, *14*, 363–368.
- (10) (a) Riplinger, C.; Neese, F. An Efficient and Near Linear Scaling Pair Natural Orbital Based Local Coupled Cluster Method. *J. Chem. Phys.* **2013**, *138*, No. 034106. (b) Riplinger, C.; Sandhoefer, B.; Hansen, A.; Neese, F. Natural Triple Excitations in Local Coupled Cluster Calculations with Pair Natural Orbitals. *J. Chem. Phys.* **2013**, *139*, No. 134101, DOI: 10.1063/1.4821834. (c) Neese, F.; Atanasov, M.; Bistoni, G.; Maganas, D.; Ye, S. Chemistry and Quantum Mechanics in 2019: Give Us Insight and Numbers. *J. Am. Chem. Soc.* **2019**, *141*, 2814–2824.
- (11) Hellweg, A.; Hättig, C.; Höfener, S.; Klopper, W. Optimized accurate auxiliary basis sets for RI-MP2 and RI-CC2 calculations for the atoms Rb to Rn. *Theor. Chem. Acc.* **2007**, *117*, 587–597.
- (12) (a) Neese, F. The ORCA Program System. *Wiley Interdiscip. Rev.: Comput. Mol. Sci.* **2012**, *2*, 73–78. (b) Neese, F. Software Update: The ORCA Program System, Version 4.0. *Wiley Interdiscip. Rev.: Comput. Mol. Sci.* **2017**, *8*, No. e1327.
- (13) Legault, C. Y. *CYLview20*; Université de Sherbrooke, 2020; <http://www.cylview.org> (accessed 24 January, 2021).
- (14) Roothaan, C. C. J. New Developments in Molecular Orbital Theory. *Rev. Mod. Phys.* **1951**, *23*, 69–89.
- (15) Hehre, W. J.; Radom, L.; Schleyer, P. v. R.; Pople, J. A. *Ab Initio Molecular Orbital Theory*; Wiley: New York, 1986.
- (16) (a) Knizia, G. Intrinsic Atomic Orbitals: An Unbiased Bridge between Quantum Theory and Chemical Concepts. *J. Chem. Theory Comput.* **2013**, *9*, 4834–4843. (b) Knizia, G.; Klein, J. E. M. N. Electron Flow in Reaction Mechanisms—Revealed from First Principles. *Angew. Chem., Int. Ed.* **2015**, *54*, 5518–5522.
- (17) (a) Perdew, J. P.; Burke, K.; Ernzerhof, M. Generalized gradient approximation made simple. *Phys. Rev. Lett.* **1996**, *77*, 3865–3868. (b) Perdew, J. P.; Burke, K.; Ernzerhof, M. Errata: Generalized gradient approximation made simple. *Phys. Rev. Lett.* **1997**, *78*, 1396.
- (18) (a) Ros, P.; Schuit, G. C. A. Molecular Orbital Calculations on Copper Chloride Complexes. *Theor. Chem. Acc.* **1966**, *4*, 1–12. (b) Lu, T.; Chen, F. Calculation of Molecular Orbital Composition. *Acta Chim. Sin.* **2011**, *69*, 2393–2406.
- (19) Johnson, E. R.; Keinan, S.; Mori-Sanchez, P.; Contreras-Garcia, J.; Cohen, A. J.; Yang, W. Revealing Noncovalent Interactions. *J. Am. Chem. Soc.* **2010**, *132*, 6498–6506.
- (20) Lu, T.; Chen, Q. Realization of Conceptual Density Functional Theory and Information-Theoretic Approach in Multiwfn Program. In *Conceptual Density Functional Theory*; WILEY-VCH GmbH: Weinheim, 2022; pp 631–647.
- (21) Lu, T.; Chen, F. Multiwfn: A Multifunctional Wavefunction Analyzer. *J. Comput. Chem.* **2012**, *33*, 580–592.
- (22) Humphrey, W.; Dalke, A.; Schulten, K. VMD: Visual molecular dynamics. *J. Mol. Graphics* **1996**, *14*, 33–38.
- (23) (a) Singleton, D. A.; Wang, Z. H. Isotope Effects and the Nature of Enantioselectivity in the Shi Epoxidation. The Importance of Asynchronicity. *J. Am. Chem. Soc.* **2005**, *127*, 6679–6685. (b) Ussing, B. R.; Hang, C.; Singleton, D. A. Dynamic Effects on the Periselectivity, Rate, Isotope Effects, and Mechanism of

Cycloadditions of Ketenes with Cyclopentadiene. *J. Am. Chem. Soc.* **2006**, *128*, 7594–7607. (c) Biswas, B.; Collins, S. C.; Singleton, D. A. Dynamics and a Unified Understanding of Competitive [2,3]- and [1,2]-Sigmatropic Rearrangements Based on a Study of Ammonium Ylides. *J. Am. Chem. Soc.* **2014**, *136*, 3740–3743. (d) Biswas, B.; Singleton, D. A. Controlling Selectivity by Controlling the Path of Trajectories. *J. Am. Chem. Soc.* **2015**, *137*, 14244–14247.

(24) (a) Yao, J.; Li, C.-L.; Fan, X.; Wang, Z.; Yu, Z.-X.; Zhao, J. Ynamide Protonation-Initiated Cis-Selective Polyene Cyclization and Reaction Mechanism. *CCS Chem.* **2022**, *4*, 2991–3001.

(b) Małosza, M. Electrophilic and Nucleophilic Aromatic Substitutions are Mechanistically Similar with Opposite Polarity. *Chem. - Eur. J.* **2020**, *26*, 15346–15353. (c) Liljenberg, M.; Stenlid, J. H.; Brinck, T. Mechanism and regioselectivity of electrophilic aromatic nitration in solution: the validity of the transition state approach. *J. Mol. Model.* **2018**, *24*, 15.

(25) Yang, Z.; Dong, X.; Yu, Y.; Yu, P.; Li, Y.; Jamieson, C.; Houk, K. N. Relationships between Product Ratios in Ambimodal Pericyclic Reactions and Bond Lengths in Transition Structures. *J. Am. Chem. Soc.* **2018**, *140*, 3061–3067.

(26) For information about Hammett constant σ_p , please see: Hansch, C.; Leo, A.; Taft, R. W. A survey of Hammett substituent constants and resonance and field parameters. *Chem. Rev.* **1991**, *91*, 165–195.

(27) Zhuo, L.-G.; Liao, W.; Yu, Z.-X. A Frontier Molecular Orbital Theory Approach to Understanding the Mayr Equation and to Quantifying Nucleophilicity and electrophilicity by Using HOMO and LUMO Energies. *Asian J. Org. Chem.* **2012**, *1*, 336–345.